submitted to Geophys. J. Int.

Sensitivity of shear-wave splitting to fracture connectivity

Yanbin He,[1] J. Germán Rubino,[2] Nicolás D. Barbosa,[3] Santiago G. Solazzi,[3] Marco Favino,[3] Tianning Chen,[1] Jinghuai Gao[4] and Klaus Holliger[3]

[1] School of Mechanical Engineering, Xi'an Jiaotong University, Xi'an, China.

[2] CONICET, Centro Atómico Bariloche - CNEA, San Carlos de Bariloche, Argentina.

Email: german.rubino@cab.cnea.gov.ar

[3] Institute of Earth Sciences, University of Lausanne, Lausanne, Switzerland.

[4] School of Information and Communications Engineering, Xi'an Jiaotong University, Xi'an, China.

23 September 2023

SUMMARY

Shear-wave splitting (SWS) is currently considered to be the most robust seismic attribute to characterize fractures in geological formations. Despite its importance, the influence of fluid pressure communication between connected fractures on SWS remains largely unexplored. Using a 3D numerical upscaling procedure based on the theory of poroelasticity, we show that fracture connectivity has a significant impact on SWS magnitude and can produce a 90° rotation in the polarization of the fast quasi-shear wave. The simulations also indicate that SWS can become insensitive to the type of fluid located within connected fractures. These effects are due to changes of fracture compliance in response to wave-induced fluid pressure diffusion. Our results improve the understanding of SWS in fractured formations and have important implications for the detection and monitoring of fracture connectivity in hydrocarbon and geothermal reservoirs as well as for the use of SWS as a forecasting tool for earthquakes and volcanic eruptions.

Key words: Shear-wave splitting; Fracture connectivity; Seismic anisotropy; Fracture and flow; Acoustic properties.

1 INTRODUCTION

The seismic method is arguably the most pertinent technique for the non-invasive detection, characterization, and monitoring of fractures in the Earth's crust, mainly because seismic waves experience velocity variation, amplitude decay, and directional dependence when propagating through fractured rocks (Liu & Martinez 2012). In particular, when a shear wave propagates through an effectively anisotropic fractured formation, it is split into two quasi-shear (qS) waves, propagating with different velocities and polarizations. This phenomenon is known as shear-wave splitting (SWS) (Crampin 1985; Crampin 2011; Volti & Crampin 2003). The time delay between these two qS-waves is typically used to infer the fracture density of the probed geological formation, whereas the polarization of the faster qS-wave contains information on the orientation of the fractures. Indeed, it is currently considered that the analysis of SWS constitutes the most robust technique to detect and characterize fracture systems (Liu et al. 2000; Liu & Martinez 2012).

Apart from applications in the context of hydrocarbon exploration and monitoring of hydraulic fracturing experiments (Baird et al. 2013; Lee & Wolf 1998; Volti & Crampin 2003), SWS has been employed to a number of pertinent problems throughout the Earth sciences. For example, temporal variations of the time delay between the qS-waves as well as a 90° flip in the polarization of the faster qS-wave are usually observed before earthquakes (Crampin et al. 2002) and volcanic eruptions (Miller & Savage 2001), thus indicating that this seismic attribute has the potential to be used as a forecasting tool (Gao & Crampin 2008).

Recent theoretical 2D analyses indicate that seismic wave velocity anisotropy and reflectivity of fractured formations can be significantly affected by the connectivity of the probed fracture network (Rubino et al. 2017; Rubino et al. 2022). The works of Rubino et al. (2017; 2022) showed that such sensitivity to fracture connectivity is a result of variations of the compliances of connected fractures in response to wave-induced fluid pressure diffusion (FPD). When a seismic wave propagates across a set of fluid-saturated fractures, the pore fluid pressure inside the fractures increases, which, in turn, counteracts the deformation.

However, if the compressed fractures are connected to others of different orientations, the fluid pressure increases are expected to be comparatively smaller, as the fluid pressure has paths to relax through flow. This FPD effect results in a temporal increase of fracture compliances, which, in turn, has a corresponding impact on the seismic velocity. The results of previous studies suggest that wave-induced FPD is expected to have an impact on SWS and, thus, this seismic attribute may contain valuable information on the connectivity degree of the probed fracture network. A few theoretical works account for wave-induced FPD in the context of seismic attenuation anisotropy and SWS, albeit only in the limit of fluid pressure equilibrium (Galvin et al. 2007; Liu et al. 2007; Sayers 2002). In most fractured geological formations and for the seismic frequency band, the equilibrium assumption may, however, not be appropriate because of the large variability of the hydraulic diffusivity in fractured formations.

In this work, we employ a numerical upscaling procedure based on the theory of poroelasticity to calculate the SWS properties of 3D models of fractured rocks in the seismic frequency band. To quantify the impact of fracture connectivity on SWS, we compare the results for samples containing either connected or unconnected conjugate fractures. The variations of SWS with respect to fracture connectivity are explored over a wide range of fracture densities and intersection angles as well as for different saturating fluids.

2 METHODOLOGICAL BACKGROUND

2.1 Model of fractured rock sample

To study the influence of fracture connectivity on SWS, we consider the computationally most effective, yet realistic scenario of an representative elementary volume (REV) with two intersecting or non-intersecting conjugate fractures embedded into a porous background (Figs 1b-d). The fractures have the same strike and are oriented at an angle $-\alpha/2$ and $\alpha/2$ with respect to the vertical, where α is a variable and refers to the fracture intersection angle. Each fracture is represented with a parallelepipedon of thickness 0.0015 m, and characterized by rectangular cross section with length and width of 0.07 m and 0.06 m, respectively. In the

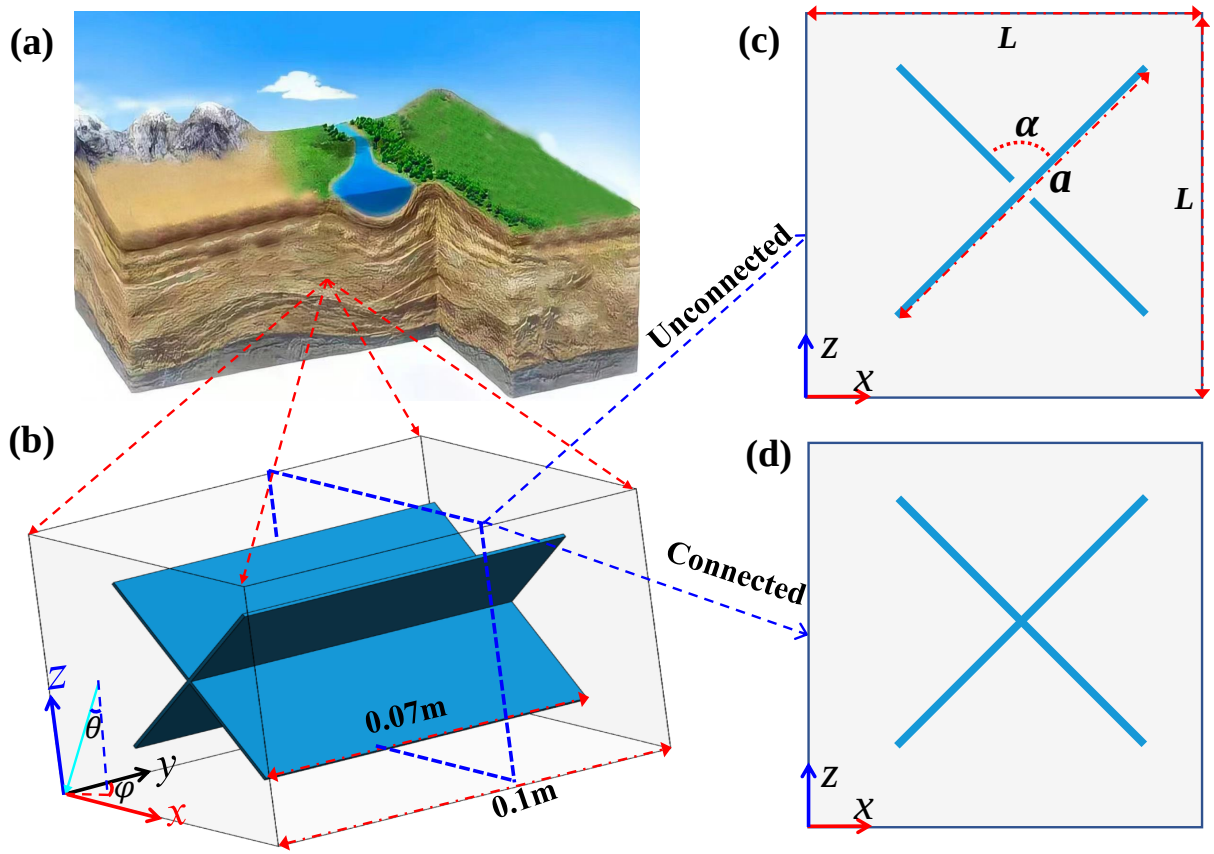

Figure 1. (a) Schematic illustration of a geological setting containing a fractured porous formation. (b) Corresponding REV characterized by conjugate fractures (blue color) embedded in a porous background (transparent gray color). Cross sections in the $x-z$ plane for (c) unconnected and (d) connected conjugate fracture models.

unconnected case, we remove a small portion of one of the fractures to avoid the intersection (Fig. 1c). In addition, the cuboid REV has a square cross section of side length L and a depth of 0.1 m. In the following, we control the fracture density (Kachanov 1992) by adjusting L while keeping the size of the fracture pair and the depth of the cuboid unchanged.

We assume that the embedding porous background corresponds to a homogeneous and isotropic tight sandstone (Rubino et al. 2017) with the following properties: solid grain bulk modulus $K_s^b = 37$ GPa, shear modulus $\mu_s^b = 44$ GPa, density $\rho_s = 2650$ kg/m^3, porosity $\phi^b = 0.05$, and permeability $\kappa^b = 10^{-20}$ m^2. The drained bulk and shear moduli are $K_m^b = 31.5$ GPa and $\mu_m^b = 37.4$ GPa, respectively. The fractures are represented as highly porous, permeable, and compliant features with $\phi^f = 0.8$, $\kappa^f = 10^{-9}$ m^2, $K_m^f = 0.04$ GPa and $\mu_m^f = 0.02$ GPa, while having the same properties at the grain level as those of the surrounding

background. Finally, we assume that both the embedding background and fractures are fully saturated with the same fluid, being either water or gas. The physical properties of water are: $K_w = 2.25$ GPa, $\rho_w = 1040$ kg/m^3, and dynamic viscosity $\eta_w = 0.001$ Pa $\cdot$ s. For gas we use: $K_g = 0.012$ GPa, $\rho_g = 78$ kg/m^3, and $\eta_g = 1.5 \times 10^{-4}$ Pa $\cdot$ s.

2.2 Numerical upscaling

To determine effective seismic signatures of fractured porous rocks accounting for FPD effects, we apply a 3D numerical upscaling procedure based on the approach proposed by Rubino et al. (2016). We consider a 3D cuboid model (Fig. 1b) as the REV of the fractured formation of interest. The fractures are represented by compliant porous inclusions characterized by high porosity and permeability, embedded in a much stiffer and much less permeable porous background (Rubino et al. 2013). Since inertial effects can be neglected for the considered frequencies, the hydromechanical behavior is governed by Biot's quasi-static poroelasticity equations (Biot 1941). To calculate the effective seismic response of the medium, we subject the REV to a series of numerical relaxation tests that allow us to retrieve an effective complex-valued and frequency-dependent Voigt stiffness matrix with 21 elements. We first apply periodic boundary conditions (BCs) on all pairs of opposite boundaries of the REV for all displacement and traction variables, and then conduct three compressibility and three shear relaxation tests. To include excitation, we modify the periodic BC for solid displacement on a given pair of boundaries by adding a time-harmonic term. For example, one of the three compressibility relaxation tests is implemented by adding a load term along the top (T) and the bottom (B) boundaries of the REV for the solid displacement variable $\mathbf{u}$ in normal direction as

$$\mathbf{u}^T \cdot \mathbf{n}^T + \mathbf{u}^B \cdot \mathbf{n}^B = -\Delta u e^{i\omega t}, \tag{1}$$

where $\mathbf{n}$ denotes the outward-directed unit normal vector, t the time and ω the angular frequency. For shear relaxation tests, the load term is added in the corresponding tangential direction.

We solve the boundary value problems using the finite-element software COMSOL Mul-

tiphysics. The model is discretized by unstructured elements, which are locally refined in the vicinity of fractures. For each test, Biot's equations of consolidation (Biot 1941) are solved by the multifrontal massively parallel sparse direct solver (MUMPS) algorithm (Amestoy et al. 2000) in the frequency domain, and the displacement variables are interpolated using the second-order Lagrange shape functions. The volume averages of the stress and strain components in response to the tests enable us to calculate an effective Voigt stiffness matrix using a least-squares procedure (Rubino et al. 2016). Finally, by solving the 3D Christoffel equation for the resulting effective viscoelastic medium (Sharma 2002), we obtain the phase velocities V_{qS1} and V_{qS2} of the two quasi-shear (qS1 and qS2) waves for different angular frequencies and angles of azimuth φ and incidence θ. Following Schubnel et al. (2003), we define the SWS parameter as

$$SWS\,(\%) = \frac{V_{qS1}\,(\omega,\theta,\varphi) - V_{qS2}\,(\omega,\theta,\varphi)}{V_{qS1}\,(\omega,\theta,\varphi)} \times 100. \tag{2}$$

As detailed in the following sections, we discriminate between qS1- and qS2-waves by their polarisation vectors with respect to the strike of the considered fractures.

3 RESULTS

3.1 Sensitivity of SWS to fracture connectivity

We first consider the case of water saturation for a wide range of fracture density from 0.01 to 0.35. We restrict ourselves to S-waves propagation along the z-axis. In this case, our numerical simulations show that the polarization of one of the qS-waves, referred to as qS1-wave, coincides with the strike of the fractures, whereas the other one, referred to as qS2-wave, is contained within the $x - z$ plane. During this initial analysis, the fracture intersection angle is set to $\alpha = 90°$. For a typical exploration seismic frequency of 30 Hz, we observe that SWS for the connected case increases and, then, decreases with fracture density for values greater than 0.22 (Fig. 2a). However, for the unconnected case (Fig. 2a), SWS always increases in magnitude but with opposite sign compared to the connected case. The contrasting behaviors indicate a strong dependence of SWS on fracture connectivity in the

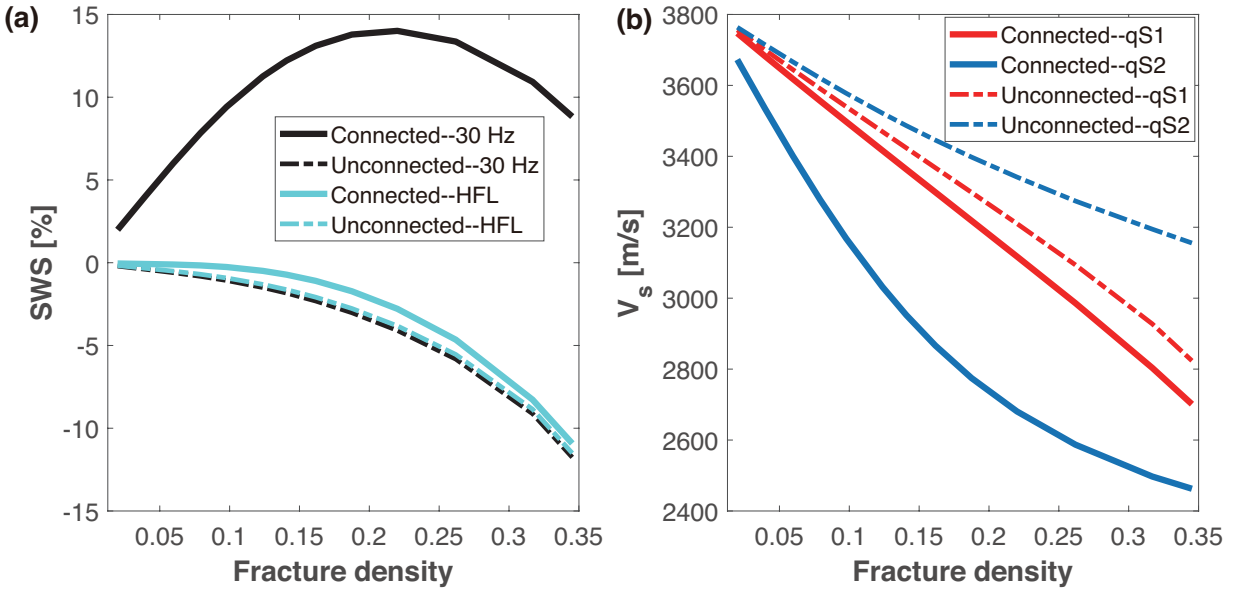

Figure 2. (a) Shear-wave splitting versus fracture density at 30 Hz and at the high-frequency limit for both the connected and unconnected fracture models shown in Fig. 1 with an intersection angle $\alpha = 90°$. (b) Variation of qS-wave velocities for both the connected and unconnected fracture models at 30 Hz.

seismic frequency range. For comparison, we also include the results in the high-frequency limit (HFL). In this case, the results of SWS for both the connected and unconnected cases are close, which implies that the significant differences in SWS observed at 30 Hz are due to wave-induced FPD within connected fractures.

Analyses of the phase velocity frequency spectrum indicate that two manifestations of FPD can occur in the considered porous rocks containing connected fractures (Rubino et al. 2013). One is FPD between the embedding background and the fractures. For low-permeability formations, the characteristic time of hydraulic diffusion in the background is typically much larger than the periods of the seismic waves, which implies that this FPD manifestation tends to prevail at frequencies below the seismic range. Indeed, for the considered tight sandstone, it occurs for frequencies around 10^{-4} Hz. The other manifestation of FPD occurs within connected fractures. The characteristic frequency is controlled by the hydraulic diffusivity, which depends on the permeability and storage coefficient of the fracture system (see Eq. (42) in Guo et al. (2009)). For hydraulically highly conductive open fractures, this manifestation of FPD tends to prevail at frequencies well above the seismic

range. For the considered model, it arises for frequencies around 10^5 Hz. For the frequency range between these two manifestations of FPD, there exists a wide plateau where neither velocity dispersion nor attenuation occurs. In the case of low-permeability formations, this non-dispersive plateau tends to cover the seismic exploration frequency band. For frequencies within this range, there is not enough time in a half wave cycle for fluid pressure communication between the fracture and background and, thus, fractures behave as hydraulically sealed with respect to the embedding medium. As a consequence, for unconnected fractures, the response is the same as that of the HFL. Conversely, in the case of the considered connected fractures, there is enough time for the fluid pressure to equilibrate within the fractures, which diminishes the stiffening effect of the saturating fluid. This hydromechanical effect alters the resulting seismic velocities and, thus, the SWS (Fig. 2a).

To further clarify the SWS differences between connected and unconnected scenarios, we investigate the dependence of the qS-wave velocities at 30 Hz on fracture density (Fig. 2b). For both the connected and unconnected cases, the velocities of the qS1-waves are similar and exhibit a quasi-linear decrease with increasing fracture density. This similar variation is expected because for the qS1-wave mode the associated shear stresses are parallel to the strike of the fracture and, hence, FPD effects are rather negligible. Conversely, compared to the qS1-wave, larger velocity differences with respect to fracture connectivity are observed for the qS2-waves. Such discrepancies occur because the associated shear stresses lie approximately in the $x - z$ plane, thus, producing maximal deformation of the fractures and, in the case of connected fractures, strong FPD effects.

3.2 Roles of fracture intersection angle and saturating fluid

We focus on a moderate fracture density of 0.1, and we again consider vertical wave propagation for a frequency of 30 Hz. When the surrounding background and the fractures are saturated by water, we observe that SWS has larger values in the connected case in comparison with the unconnected one, particularly for intermediate intersection angles (Fig. 3). When the intersection angle approaches 90 degrees, the vertically-propagating qS2-wave

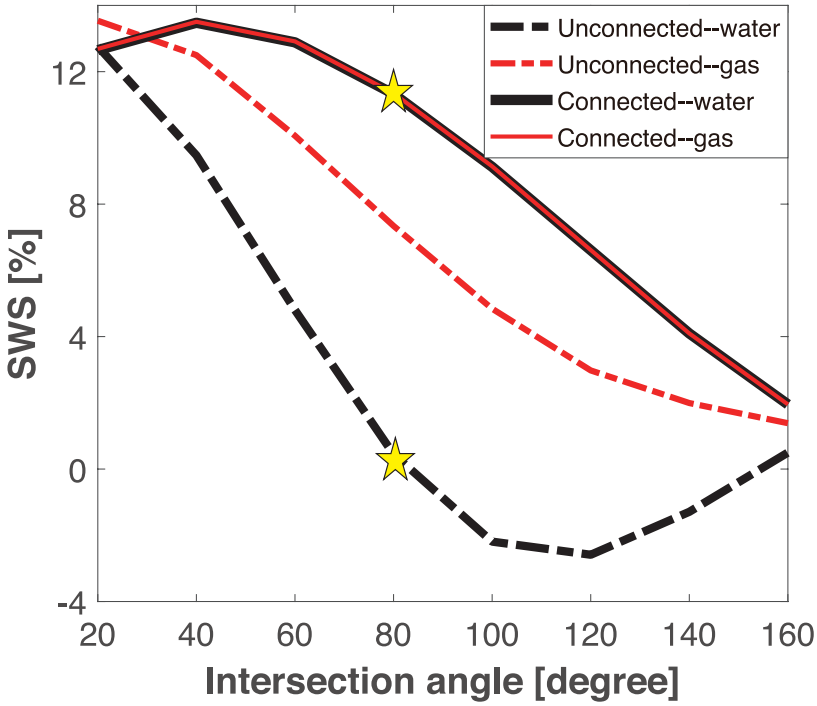

Figure 3. SWS as a function of fracture intersection angle α for either water (black lines) or gas (red lines) saturation. Yellow stars denote the SWS in a water saturated medium for both connected and unconnected scenarios and for $\alpha = 80°$.

induces maximum increase of fluid pressure in one fracture set, while it produces maximum decrease in the remaining fractures having opposite orientation (Rubino et al. 2017). The resultant fluid pressure gradients can be released in the connected case, thus producing maximum discrepancies with respect to the unconnected one. However, when the intersection angle approaches 0 or 180 degrees, the two fractures of the REV are almost parallel. Consequently, both fractures are almost equally affected by the passing wave, and it does not matter whether they are connected or not, as there are no strong fluid pressure gradients to equilibrate.

We observe that, in the unconnected case, the SWS curves for water and gas saturations are clearly different (Fig. 3). Conversely, when fractures are connected, the SWS parameter is independent of the saturating fluid. In the considered seismic frequency range, the reduction of the stiffening effect of the fluid contained within connected fractures in response to FPD makes them behave as if they were drained and, therefore, the response turns out to be virtually insensitive to the type of pore fluid. This characteristic of SWS with respect to

saturating fluids provides a diagnostic feature to detect fracture connectivity but also makes the identification of the saturating fluid potentially more difficult. Therefore, using multi-component seismic information could be a promising avenue to infer more accurately both fracture connectivity and the type of saturating fluids.

4 DISCUSSION AND CONCLUSIONS

The main result of this work is that fracture connectivity influences significantly shear-wave splitting (SWS) throughout the seismic frequency range. This effect is due to wave-induced fluid pressure diffusion (FPD) within connected fractures and cannot be accounted for using classical effective medium models. Our simulations thus indicate that SWS inherently contains information on the effective hydraulic properties of the probed fractured formations.

Caspari et al. (2018) compared the results of poroelastic wave propagation simulations to those obtained with the effective numerical upscaling approach used in this study. While their work confirms the basic consistence between these two approaches, it also illustrates that accounting for mesoscopic FDP in explicit wave propagation simulations is technically challenging and computationally immensely costly due to the vast differences in scale between the prevailing diffusion and wave phenomena. In view of this, and given the additional challenges associated with the 3D nature of our work, we decided to use the numerical upscaling approach. However, from a practical point of view, it is important to remark that a reservoir-scale model can then be populated with the inferred effective media, and synthetic seismograms can be obtained by numerical simulations of seismic wave propagations through the resulting anisotropic viscoelastic medium. In this sense, and to illustrate the impact of fracture connectivity on seismic waveforms, we consider a cubic reservoir model with a side length of 2.5 km (Fig. 4a), whose properties correspond to a homogeneous viscoelastic medium obtained from the upscaled REV containing either connected or unconnected fracture networks. We assume that the fractures are water-saturated having an intersection angle $\alpha = 80^\circ$ (yellow stars in Fig. 3) and the fracture density is 0.1. The physical domain of the model is surrounded by absorbing layers to set up effective nonreflecting-like boundary

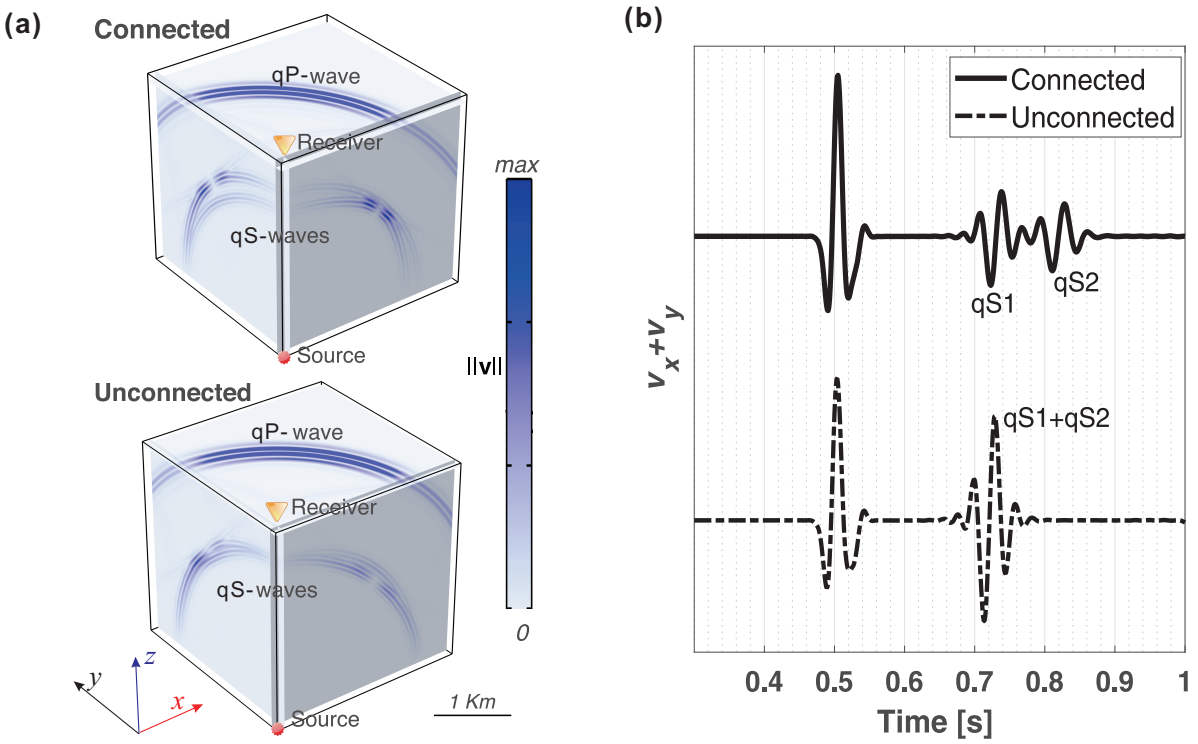

Figure 4. (a) Snapshots, taken at 0.6 s, of particle velocity magnitude associated with the propagation of seismic waves through a fractured formation containing either connected or unconnected fractures. The source and receiver are denoted by the red circle and golden triangle, respectively. (b) Synthetic seismic traces of the particle velocity $(v_x + v_y)$ recorded by the receiver.

conditions. A directional Ricker-type force source is imposed in the model (red circle in Fig. 4a). The central frequency of the source is 30 Hz and the time delay is 0.03 s. We employ a discontinuous Galerkin method (COMSOL Multiphysics) to solve the elastic wave equations in the velocity-strain formulation. The model is discretized using hexahedron elements with more than three cells per shortest dominant wavelength, and the classical fourth-order Runge-Kutta method is employed for time-stepping to solve the problem in the time domain explicitly.

Fig. 4 shows snapshots of the particle velocity magnitude at a propagation time of 0.6 s. The response of the qP-wave is essentially identical in both connected and unconnected cases. Conversely, the responses of the qS-waves are significantly different for the two scenarios. Particularly, in the connected case, the SWS phenomenon is more pronounced. Seismic traces of the particle velocity $(v_x + v_y)$ recorded by the receiver (golden triangle in Fig. 4a) are

illustrated in Fig. 4b. In the unconnected case, the qS-waves overlap, while they are clearly separated in the presence of connected fractures. This observation is in good agreement with the variation of the SWS parameter shown in Fig. 3. The snapshots together with the seismic traces shown in Fig. 4 further demonstrate that the connectivity of the fractures has a significant impact on the SWS, which, according to our results, could be observed in seismic signals.

Due to the computational cost of 3D modeling, we restricted our study to a regular distribution of conjugate pairs of connected or unconnected fractures. In these cases, wave-induced FPD within connected fractures is responsible for the sensitivity of SWS to fracture connectivity for low fracture densities. Given the periodicity of our fracture distribution, mechanical interactions play an important role for relatively high fracture densities, as can be seen by the change in the SWS curves for fracture densities above 0.22 (Fig. 2a). In most natural fractured reservoirs, fracture densities typically correspond to the dilute fracture regime and fractures are more likely to be randomly distributed (Gurevich et al. 2009). Mechanical interactions between fractures tend to be effectively cancelled out and, thus, FPD effects should be dominant. Consequently, fracture connectivity is expected to manifest as significant changes in the magnitude and sign of SWS. Variations of SWS are expected to depend on the degree of connectivity of the probed fracture system as well as on the effective fracture orientation (Liu et al. 2006) relative to the angles of incidence and azimuth. The analysis of more realistic fracture networks and different degrees of fracture connectivity is beyond our current computational capabilities.

Orthogonal rotation in polarization of the fast qS-wave is a distinct characteristic widely observed in the context of earthquakes, volcanic eruptions, and hydraulic fracturing. The orthogonal rotation has been ascribed to the coalescence of microcracks into larger fractures as the system develops towards fracture criticality (Crampin 2011) under high fluid pressure. In this sense, hydraulic fracturing increases the fracture density and decreases the aspect ratio, generating longer and better connected fractures (Usher et al. 2017). In the seismic exploration frequency range, our results show that the SWS parameters exhibit opposite

signs for connected and unconnected fractures (Fig. 2a), which, based on the corresponding definition in Eq. (2), indicates an orthogonal rotation in the polarization of the fast qS-wave. When fractures are connected, the polarization of the fast shear wave (qS1) is parallel to the direction of fracture strike (Fig. 2b). However, for the unconnected fracture model, the fast shear wave corresponds to the qS2-mode, for which the polarization direction is within the plane orthogonal to the fracture strike. Moreover, the results indicate that these SWS changes cannot be explained if wave-induced FPD is neglected. Our study provides quantitative evidence that orthogonal rotation in the fast qS-wave polarization may be due to changes in fracture connectivity, which introduces a new perspective for understanding and interpreting SWS variations in fractured formations.

ACKNOWLEDGMENTS

J. G. R. acknowledges the financial support from CONICET (PIP 11220210100346CO). The contributions of N. D. B., M. F., and K. H. benefited from Swiss National Science Foundation grants 196037, 180112, and 178946, respectively. This project has received funding from the European Union's HORIZON 2020 research and innovation programme under the Marie Sktodowska-Curie grant agreement No. 101007851. The work was also supported by the Chinese Scholarship Council (202006280416).

DATA AVAILABILITY

The data associated with this paper are available at https://doi.org/10.5281/zenodo.7132147.

REFERENCES

Amestoy, P.R., Duff, I.S. & L'excellent, J.Y., 2000. Multifrontal parallel distributed symmetric and unsymmetric solvers, Comput. Methods. Appl. Mech. Eng., 184, 501-520.

Baird, A.F., Kendall, J.M., Verdon, J.P., Wuestefeld, A., Noble, T.E., Li, Y., Dutko, M. & Fisher, Q.J., 2013.Monitoring increases in fracture connectivity during hydraulic stimulations from temporal variations in shear wave splitting polarization, Geophys. J. Int., 195, 1120-1131.

Biot, M.A., 1941. General theory of three-dimensional consolidation, J. Appl. Phys., 12, 155-164.

Caspari, E., Novikov, M., Lisitsa, V., Barbosa, N. D., Quintal, B., Rubino, J. G., & Holliger, K., 2018. Attenuation mechanisms in fractured fluid-saturated porous rocks: a numerical modelling study, Geophys. Prospect., 67, 935-955.

Crampin, S., 1985. Evaluation of anisotropy by shear-wave splitting, Geophysics, 50, 142-152.

Crampin, S., 2011. Shear-wave Splitting: New geophysics and earthquake stress-forecasting, Encyclopedia of Solid Earth Geophysics, 2, 1355-1362, Springer, Heidelberg.

Crampin, S., Volti, T., Chastin, S., Gudmundsson, A. & Stefansson, R., 2002. Indication of high pore-fluid pressures in a seismically-active fault zone, Geophys. J. Int., 151, F1-F5.

Galvin, R.J., Gurevich, B. & Sayers, C.M., 2007. Fluid-dependent shear-wave splitting in a poroelastic medium with conjugate fracture sets, Geophys. Prospect., 55, 333-343.

Gao, Y. & Crampin, S., 2008. Shear-wave splitting and earthquake forecasting, Terra Nova, 20, 440-448.

Guo, J., Rubino, J. G., Glubokovskikh, S. & Gurevich, B., 2017. Effects of fracture intersections on seismic dispersion: theoretical predictions versus numerical simulations, Geophys. Prospect., 65, 1264-1276.

Gurevich, B., Brajanovski, M., Galvin, R.J., Müller, T.M. & Toms-Stewart, J., 2009. P-wave dispersion and attenuation in fractured and porous reservoirs–poroelasticity approach, Geophys. Prospect., 57, 225-237.

Kachanov, M., 1992. Effective Elastic Properties of Cracked Solids: Critical Review of Some Basic Concepts, Appl. Mech. Rev., 45, 304-335.

Lee, M.K. & Wolf, L.W., 1998. Analysis of fluid pressure propagation in heterogeneous rocks: Implications for hydrologically-induced earthquakes, Geophys. Res. Lett., 25, 2329-2332.

Liu, E., Chapman, M., Varela, I., Li, X., Queen, J. H. & Lynn, H., 2007. Velocity and attenuation anisotropy: Implication of seismic fracture characterizations, The Leading Edge, 26, 1170-1174.

Liu, E., Chapman, M., Zhang, Z. & Queen, J. H., 2006. Frequency-dependent anisotropy: Effects of multiple fracture sets on shear-wave polarizations, Wave Motion, 44, 44-57.

Liu, E., Hudson, J.A. & Pointer, T., 2000. Equivalent medium representation of fractured rock, J. Geophys. Res., 2981–3000.

Liu, E. & Martinez, A., 2012. Seismic Fracture Characterization: Concepts and Practical Applications, EAGE.

Miller, V. & Savage, M., 2003. Changes in seismic anisotropy after volcanic eruptions: evidence from Mount Ruapehu, Science, 293, 2231-2233.

Rubino, J.G., Barbosa, N., Hunziker, J. & Holliger, K., 2022. Can we use seismic reflection data to infer the interconnectivity of fracture networks?, Geophys. J. Int., 231, 996-1010.

Rubino, J.G., Caspari, E., Müller, T.M., Milani, M. Barbosa, N. & Holliger, K., 2016. Numerical

upscaling in 2D heterogeneous poroelastic rocks: Anisotropic attenuation and dispersion of seismic waves, J. Geophys. Res., 121, 6698–6721.

Rubino, J.G., Caspari, E., Müller, T.M., Milani, M. & Holliger, K., 2017. Fracture connectivity can reduce the velocity anisotropy of seismic waves, Geophys. J. Int., 210, 223-227.

Rubino, J.G., Guarracino, L., Müller, T.M. & Holliger, K., 2013. Do seismic waves sense fracture connectivity?, Geophys. Res. Lett., 40, 692-696.

Sayers, C.M., 2002. Fluid-dependent shear-wave splitting in fractured media, Geophys. Prospect., 50, 393-401.

Schubnel, A. &Guéguen, Y., 2003. Dispersion and anisotropy of elastic waves in cracked rocks, J. Geophys. Res., 108, 2101.

Sharma, M.D., 2002. Group velocity along general direction in a general anisotropic medium, Int. J. Solids. Struct., 39, 3277-3288.

Usher, P.J., Kendall, J.M., Kelly, C.M. & Rietbrock, A., 2017. Measuring changes in fracture properties from temporal variations in anisotropic attenuation of microseismic waveforms, Geophys. Prospect., 65, 347–362.

Volti, T. & Crampin, S., 2003. A four-year study of shear-wave splitting in Iceland: 2. Temporal changes before earthquakes and volcanic eruptions, Geol. Soc. Lond. Spec. Publ., 212, 135-149.